OPTIMAL CONTROL APPLICATIONS AND METHODS
Optim. Control Appl. Meth., 2002; **23**:215–238 (DOI: 10.1002/oca.711)

Numerical optimization study of multiple-pass aeroassisted orbital transfer

Anil V. Rao*,†,‡, Sean Tang§,¶ and Wayne P. Hallman‖,**

The Aerospace Corporation, El Segundo, CA 90245-4691, U.S.A.

SUMMARY

A direct transcription method is applied to the problem of multiple-pass aeroassisted orbital transfer from geostationary orbit to low Earth orbit with a large inclination change. The objective is to provide minimum-impulse requirements and corresponding optimal trajectories for a gliding vehicle with a high lift-to-drag ratio subject to constraints on heating rate, angle of attack, and transfer time. The multiple-pass aeroassisted orbital transfer problem is set up as a multi-phase optimal control problem. All relevant parameters, including de-orbiting, intermediate, and circularizing impulses, are optimized. Copyright © 2002 John Wiley & Sons, Ltd.

KEY WORDS: optimal trajectories; astrodynamics; orbital transfer; numerical methods; multiple-pass aeroassisted orbital maneuvers

INTRODUCTION

It is well known that using aerodynamic forces to change the inclination of the orbit of a spacecraft can significantly reduce propellant expenditure compared to exo-atmospheric all-propulsive maneuvers. The two most widely studied types of the so-called synergetic maneuvers are aeroglide and aerocruise. The former uses only aerodynamic forces whereas the latter includes continuous thrusting during the atmospheric segment of the trajectory. In this paper, we are interested in aerogliding maneuvers for a high lift-to-drag vehicle.

The problem of aeroassisted orbital transfer has received a great deal of attention. Much of the early work is summarized in the surveys of References [1, 2]. More recent studies on

*Correspondence to: Dr. Anil V. Rao, Charles Stark Draper Laboratory, Inc., 555 Technology Square, Mail Stop 70, Cambridge, MA 02139-3563, U.S.A.
† E-mail: anilvrao@alumni.princeton.edu
‡ Senior Member of the Technical Staff, Flight Mechanics Department.
§ Senior Member of the Technical Staff, Flight Mechanics Department.
¶ E-mail: sean.tang@aero.org
‖ Director, Flight Mechanics Department.
** E-mail: wayne.hallman@aero.org

Contract/grant sponsor: United States Air Force Space and Missile Systems Center

Received 26 September 2000
Revised 28 May 2002
Accepted 3 June 2002

aeroassisted orbital transfer with inclination change can be found in References [3, 4]. Seywald [5] has presented optimal aeroglide trajectories for an aeroassisted orbital transfer vehicle subject to a heating rate constraint. Lee and Hull [6] have obtained optimal solutions for an aerocruise maneuver and an aeroglide maneuver with a thrusting phase that is constrained to maximum thrust.

Due to the complexity of the atmospheric maneuvers, aeroassisted orbital transfer problems are generally formulated as optimal control problems. Moreover, because these optimal control problems generally cannot be solved analytically, it is necessary to obtain solutions numerically. Numerical methods for solving optimal control problems are classified as either indirect or direct. Indirect methods involve determining extremals by solving the Hamiltonian boundary-value problem (HBVP) posed by the first-order optimality condition. Direct methods involve transcribing the optimal control problem to a non-linear programming (NLP) by parameterizing the state and control. The NLP is then solved using a numerical optimization method.

In many aeroassisted orbital transfer studies, the optimal control problems have been solved using indirect methods [5, 7, 8]. Indirect methods have the advantage over direct methods that they offer a great deal of insight into the structure of the optimally controlled system. Furthermore, satisfying the necessary conditions for optimality is greater evidence that an optimal solution has been found as compared with obtaining convergence from a non-linear programming routine. Using indirect methods, a great deal of understanding about the problem of aeroassisted orbital transfer has been obtained. However, it is important to point out that this understanding has been limited because it has not been possible to obtain solutions to the HBVPs that arise from the first-order necessary conditions due to extreme sensitivity of the HBVPs to unknown boundary conditions. In some cases this extreme sensitivity has been overcome and numerical solutions have been obtained by making drastic modelling simplifications. However, in order to obtain realistic solutions it has often not been possible to simplify the HBVPs and hence it has not been possible to obtain numerical solutions.

In recent years, direct methods for solving optimal control problems have risen to prominence [9–12]. Direct methods have the advantage over indirect methods that they are capable of solving a much wider range of problems, are more robust to relatively large errors in the initial guess, and are more computationally efficient. Examples of software that employ direct methods include the programs *Optimal Trajectories by Implicit Simulation* (OTIS) [13], *Graphical Environment for Solving Optimal Control Problems* (GESOP) [14] and *Sparse Optimal Control Software* (SOCS) [15]. Several studies have already been performed to demonstrate the effectiveness of direct methods for solving problems in aeroassisted orbital transfer. In particular, a direct transcription method has been applied to the aeroglide and aerocruise problem of low Earth orbit (LEO) to LEO aeroassisted orbital transfer with small inclination change using a single atmospheric flight segment [16]. The results demonstrate clearly that the use of direct methods will greatly enhance the understanding of the problem of aeroassisted orbital transfer.

The goal of this research is to gain a better understanding of the performance requirements and the structure of trajectories for minimum-impulse aerogliding maneuvers with a large required inclination change using a *direct* return from high Earth orbit (HEO) to LEO (a direct return from HEO to LEO is one where the size of the orbit decreases on the transfer trajectory). An important difference between small inclination LEO to LEO aeroassisted orbital transfer and large inclination HEO to LEO aeroassisted orbital transfer is that the heating incurred

during an atmospheric pass in the former is significantly less than that of the latter. More specifically, because of heating limitations, it will generally not be possible to perform a large inclination HEO to LEO transfer in a single pass. Consequently, multiple atmospheric passes will be required to accomplish the transfer.

In this paper, accurate numerical solutions are presented to the problem of minimum-impulse multiple-pass aerogliding maneuvers for a high lift-to-drag vehicle with constraints on heating rate for the case of a *direct* return from geostationary orbit (GEO) to LEO. For completeness it is mentioned that, while it is possible to obtain lower fuel consumption by initially increasing the size of the orbit of the vehicle (see Reference [17]) or by including a lunar swing-by, these possibilities are not included in this study because of operational constraints (e.g. limits on transfer time). The multiple-pass aeroassisted orbital transfer problem is formulated as a multi-phase optimal control problem. The optimal control problem is solved using the numerical optimal control software SOCS [15]. The performance is assessed as a function of (1) the number of atmospheric passes; (2) the maximum allowable heating rate and (3) the required inclination change.

It is shown that the multiple-pass aeroassisted orbital transfer offers little to no savings in total impulse over the single-pass transfer when the heating rate is unconstrained but offers significant savings in total impulse when the heating rate is constrained. Moreover, the incremental advantage of the multiple-pass transfer diminishes as the number of atmospheric passes increases. It is also shown that the aeroassisted orbital transfer offers significant savings in total impulse over all-propulsive transfers. An interesting feature of the approach developed here is that the optimal split between atmospheric and impulsive inclination change is determined. In particular, a limit is found to the total amount of inclination change performed during atmospheric flight. Finally, a particular case of a four-pass transfer is used to illustrate the main features common to all of the optimal trajectories.

PHYSICAL MODEL AND EQUATIONS OF MOTION

Two dynamic models are used for the aeroassisted orbital transfer vehicle (AOTV): one for space flight and one for atmospheric flight. During space flight, the motion of the AOTV is assumed to be Keplerian with the exception of impulsive thrust maneuvers that model instantaneous changes in velocity (ΔV). The orbit propagation is done using the analytic propagator of Reference [18]. The model for the impulsive thrust is

$$\Delta V = g_0 I_{\mathrm{sp}} \ln \frac{m_1}{m_2} \tag{1}$$

where m_1 and m_2 are the vehicle masses before and after the application of the impulse, respectively.

During atmospheric flight, the AOTV is modeled as a point mass that flies unpowered over a spherical non-rotating Earth under the influence of aerodynamic forces. The aerodynamic model is taken from Reference [16] and represents a high lift-to-drag delta wing vehicle. The

drag acceleration, D, and lift acceleration, L, are given as

$$\begin{aligned} D &= qSC_{\mathrm{D}}/m \\ L &= qSC_{\mathrm{L}}/m \end{aligned} \tag{2}$$

where $q = \rho v^2/2$. The model for the coefficient of drag is

$$C_{\mathrm{D}} = C_{\mathrm{D}_0} + KC_{\mathrm{L}}^2 \tag{3}$$

The differential equations describing the motion of the AOTV during atmospheric flight are given in spherical co-ordinates [19] as

$$\begin{aligned} \frac{\mathrm{d}r}{\mathrm{d}t} &= v\sin\gamma \\ \frac{\mathrm{d}\theta}{\mathrm{d}t} &= \frac{v\cos\gamma\cos\psi}{r\cos\phi} \\ \frac{\mathrm{d}\phi}{\mathrm{d}t} &= \frac{v\cos\gamma\sin\psi}{r} \\ \frac{\mathrm{d}v}{\mathrm{d}t} &= -D - g\sin\gamma \\ \frac{\mathrm{d}\gamma}{\mathrm{d}t} &= \frac{1}{v}\left[L\cos\sigma - \left(g - \frac{v^2}{r}\right)\cos\gamma\right] \\ \frac{\mathrm{d}\psi}{\mathrm{d}t} &= \frac{1}{v}\left[\frac{L\sin\sigma}{\cos\gamma} - \frac{v^2}{r}\cos\gamma\cos\psi\tan\phi\right] \end{aligned} \tag{4}$$

where $g = \mu/r^2$. The angle of attack, α, is computed from C_{L} as

$$\alpha = C_{\mathrm{L}}/C_{\mathrm{L},\alpha} \text{ with } C_{\mathrm{L},\alpha} = \text{constant} \tag{5}$$

where $C_{\mathrm{L}} \in \left[0, C_{\mathrm{L,\,max}}\right]$ and $C_{\mathrm{L,\,max}} = 0.4$. The value of $C_{\mathrm{L,\,max}} = 0.4$ corresponds to an angle of attack $\alpha \approx 40^\circ$, beyond which lift is lost. Furthermore, the altitude of the AOTV is computed over a spherical Earth as

$$h = r - R_{\mathrm{e}} \tag{6}$$

It is assumed in this study that the *sensible* atmosphere (i.e. that which can be sensed by accelerometers on board the vehicle) lies between altitudes of zero and 60 nm. Therefore, the transition between space flight and atmospheric flight occurs at an altitude of 60 nm. Finally, the model used for air density is a smoothed 1962 U.S. Standard Atmosphere [20]. Table I shows the numerical values of all constants used in the simulations.

Table I. Aerodynamic data, vehicle data, and physical data for aeroassisted orbit transfer problem

Quantity	Numerical value
m_0	519.5 slug
m_e	156.5 slug
I_{sp}	310 s
R_e	20 926 430 ft
μ	1.40895×10^{16} ft^3/s^2
ρ_e	0.0023769 slug/ft^3
S	125.84 ft^2
C_{D_0}	0.032
K	1.4
$C_{L,\alpha}$	0.5699

PATH CONSTRAINTS

During atmospheric flight, inequality path constraints are imposed on the stagnation point heating rate, $dQ/dt \equiv \dot{Q}$, and the coefficient of lift, C_L. The stagnation point heating rate is computed using the equation [21]

$$\dot{Q} = 17\,600(\rho/\rho_e)^{0.5}(v/v_e)^{3.15}\text{BTU}/(\text{ft}^2\,\text{s}) \tag{7}$$

Denoting the maximum allowable stagnation point heating rate during atmospheric flight by $\dot{Q}_{max}$, the following two constraints are imposed during atmospheric flight:

$$C_L \leqslant C_{L,\,max} \tag{8}$$

$$\dot{Q} \leqslant \dot{Q}_{max} \tag{9}$$

PARAMETERIZATION OF CONTROL

When solving path constrained optimal control problems using a direct transcription method, the path constraint index plays a crucial role in determining the solution accuracy [22, 23]. Given a choice of different control parameterizations, it is preferable to choose one where the path constraint index is as low as possible (see References [22, 23] for a detailed discussion of path constraint index). Using $[C_L \;\; \sigma]$ as the control, the path constraint of Equation (9) is index three. However, if the control $[u_1 \;\; u_2]$ is used where

$$\begin{aligned} u_1 &= -C_L \sin\sigma \\ u_2 &= -C_L \cos\sigma \end{aligned} \tag{10}$$

the index of the path constraint of Equation (9) is lowered from three to two. Consequently, using the control $[u_1 \;\; u_2]$ is preferable to using the control $[C_L \;\; \sigma]$. In terms of u_1 and u_2, Equation

(4) can be written as

$$\begin{aligned}
\frac{\mathrm{d}r}{\mathrm{d}t} &= v\sin\gamma \\
\frac{\mathrm{d}\theta}{\mathrm{d}t} &= \frac{v\cos\gamma\cos\psi}{r\cos\phi} \\
\frac{\mathrm{d}\phi}{\mathrm{d}t} &= \frac{v\cos\gamma\sin\psi}{r} \\
\frac{\mathrm{d}v}{\mathrm{d}t} &= -D - g\sin\gamma \\
\frac{\mathrm{d}\gamma}{\mathrm{d}t} &= \frac{1}{v}\left[-\frac{qS}{m}u_2 - \left(g - \frac{v^2}{r}\right)\cos\gamma\right] \\
\frac{\mathrm{d}\psi}{\mathrm{d}t} &= \frac{1}{v}\left[\frac{-qS}{m\cos\gamma}u_1 - \frac{v^2}{r}\cos\gamma\cos\psi\tan\phi\right]
\end{aligned} \tag{11}$$

where the set of admissible controls is given as

$$\mathscr{U} = \left\{(u_1, u_2):\ \sqrt{u_1^2 + u_2^2} \leqslant C_{\mathrm{L,\,max}}\right\} \tag{12}$$

The variables C_{L} and σ are then computed *a posteriori* from u_1 and u_2 as

$$\begin{aligned}
C_{\mathrm{L}} &= \sqrt{u_1^2 + u_2^2} \\
\sigma &= \tan^{-1}(u_1/u_2)
\end{aligned} \tag{13}$$

where $\tan^{-1}$ is the four-quadrant inverse tangent.

PROBLEM FORMULATION

Consider the problem of transferring an AOTV from a geostationary (GEO) orbit to LEO using a fixed number of atmospheric passes via a *direct* return from GEO. Let the vehicle mass in the initial geostationary orbit and the vehicle empty mass be denoted by m_0 and m_{e}, respectively. The initial state at time $t_0 = 0$ is given in terms of orbital elements as

$$\begin{aligned}
h_{\mathrm{a}}(t_0) &= 19\,323\ \mathrm{nm} \\
h_{\mathrm{p}}(t_0) &= 19\,323\ \mathrm{nm} \\
i(t_0) &= 0^\circ \\
\omega(t_0) &= 0^\circ \\
\tau(t_0) &= 0^\circ \\
\Omega(t_0) &= 0^\circ
\end{aligned} \tag{14}$$

Since the initial orbit is circular and equatorial, v, ω, and Ω can be chosen arbitrarily. Table I gives the values of all relevant quantities used in the simulations where the quantity R_e denotes the radius of the Earth and the value of I_{sp} corresponds to a vehicle with a high thrust engine capable of delivering a total impulse of 12 000 ft/s.

TRAJECTORY EVENT SEQUENCE

Let the number of atmospheric passes for a given orbital transfer be denoted by n. The trajectory event sequence for an n-pass transfer is divided into $n+1$ phases as follows. The event sequence for phase 1 is given as

(i) de-orbit impulse of magnitude ΔV_1 from the initial condition of (14);
(ii) space flight segment that starts at apogee of the geostationary transfer orbit (after the application of ΔV_1) and terminates at atmospheric entry and
(iii) atmospheric flight segment that starts at the first atmospheric entry and terminates at the first atmospheric exit.

The event sequence for phase i, $i = 2, \ldots, n$ is given as

(i) space flight segment that starts at the $(i-1)$th atmospheric exit and terminates at apogee of the $(i-1)$th intermediate orbit;
(ii) impulse ΔV_i at the apogee of the $(i-1)$th intermediate orbit;
(iii) space flight segment that starts at the state following the application of ΔV_i and terminates at the ith atmospheric entry and
(iv) atmospheric flight segment that starts at the ith atmospheric entry and terminates at the ith atmospheric exit.

The event sequence for phase $n+1$ is given as

(i) space flight segment that starts at the nth atmospheric exit and terminates at apogee of the final orbit;
(ii) circularizing impulse ΔV_{n+1} at apogee of the final orbit.

The event sequences for phases $1, \ldots, n+1$ are drawn schematically in Figures 1–3.

In all simulations, the directions of the initial de-orbit impulse ΔV_1 and the intermediate impulses $\Delta V_2, \ldots, \Delta V_n$ are determined via Euler pitch angles of 180° and Euler yaw angles χ_1 and $\chi_2, \ldots, \chi_n$, respectively, while the direction of the final circularizing impulse ΔV_{n+1} is fixed. The Euler angles for impulses $\Delta V_2, \ldots, \Delta V_n$ are measured in a velocity reference frame whose principal directions $\mathbf{e}_1$, $\mathbf{e}_2$, and $\mathbf{e}_3$ are given as

$$\begin{aligned} \mathbf{e}_1 &= \boldsymbol{v}/v \\ \mathbf{e}_2 &= \frac{\boldsymbol{r} \times \mathbf{e}_1}{\|\boldsymbol{r} \times \mathbf{e}_1\|} \\ \mathbf{e}_3 &= \mathbf{e}_1 \times \mathbf{e}_2 \end{aligned} \tag{15}$$

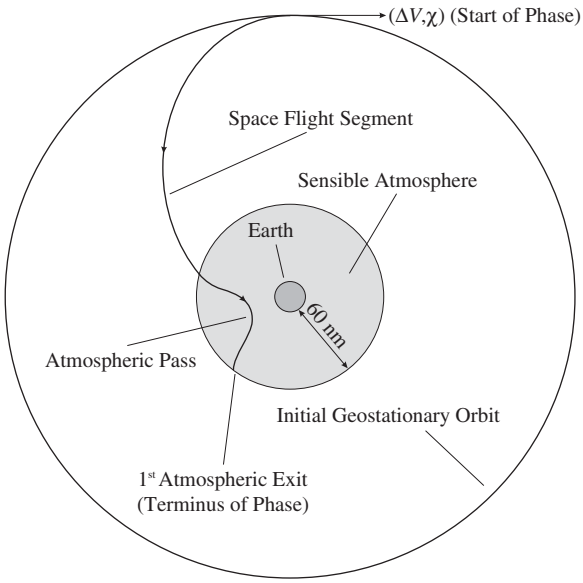

Figure 1. Schematic of phase 1 of n-pass aeroassisted orbital transfer problem.

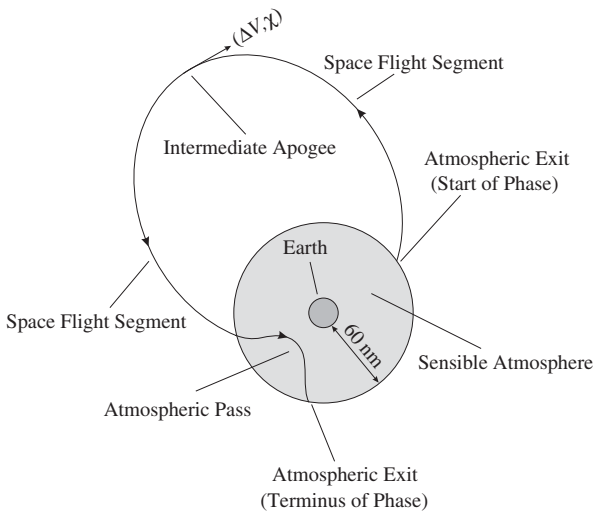

Figure 2. Schematic of phases $i = 2, \ldots, n$ of n-pass aeroassisted orbital transfer problem.

where $\|\cdot\|$ denotes the vector 2-norm. It is noted that, while the minimum impulse may decrease slightly if the direction of the final circularizing impulse ΔV_{n+1} is allowed to vary, this decrease will be quite small and will have a relatively insignificant affect on the overall performance.

The space flight segments before and after the application of $\Delta V_i, i = 1, \ldots, n+1$ are denoted s_i^- and s_i^+, respectively, and have angular lengths $\Delta\tau_i^-$ and $\Delta\tau_i^+$, respectively. The angles $\Delta\tau_i^-$ and

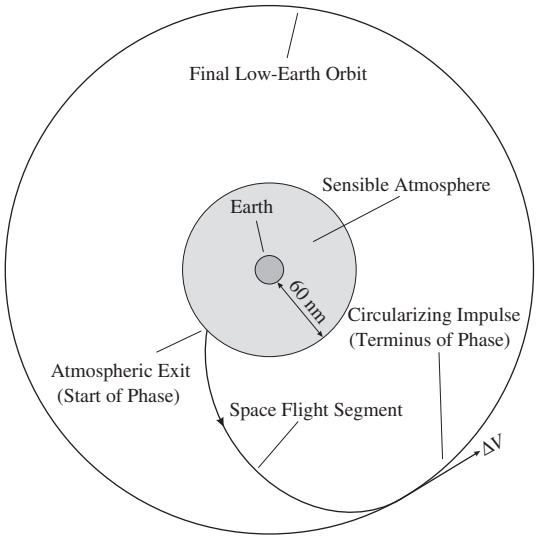

Figure 3. Schematic of phase $n+1$ of n-pass aeroassisted orbital transfer problem.

$\Delta\tau_i^+$ correspond to changes in true anomaly of the Keplerian orbit (note that s_1^- and s_{n+1}^+ are both space flight segments of length zero since there is neither propagation prior to the application of ΔV_1 nor subsequent to the application of ΔV_{n+1}).

INTERIOR POINT CONSTRAINTS AND BOUNDARY CONDITIONS

To force the AOTV to enter the sensible atmosphere, the altitudes after the space flight segments $s_i^+, i=1,\ldots,n$ are constrained to the atmospheric limit of 60 nm. To ensure continuity, the states and times after the space flight segments $s_i^+, i=1,\ldots,n$ are forced to match the states and times at the corresponding atmospheric entries. Denoting the time at the end of the space flight segment s_i^+ and the time of the ith atmospheric entry by t_i^+ and $t_{\text{entry},\,i}$, respectively, the following equality constraints are enforced at all n atmospheric entries:

$$\left.\begin{aligned} t_i^+ &= t_{\text{entry},\,i} \\ h(t_{\text{entry},\,i}) &= 60\ \text{nm} \\ h(t_i^+) &= h(t_{\text{entry},\,i}) \\ \theta(t_i^+) &= \theta(t_{\text{entry},\,i}) \\ \phi(t_i^+) &= \phi(t_{\text{entry},\,i}) \\ v(t_i^+) &= v(t_{\text{entry},\,i}) \\ \gamma(t_i^+) &= \gamma(t_{\text{entry},\,i}) \\ \psi(t_i^+) &= \psi(t_{\text{entry},\,i}) \end{aligned}\right\}, \quad i=1,\ldots,n \tag{16}$$

Similarly, the ith atmospheric flight segment ends when the vehicle re-attains an altitude of 60 nm. Denoting the time of the ith atmospheric exit and the time of the beginning of the space flight segment s_i^- by $t_{\text{exit},\,i}$ and t_i^-, respectively, the following equality constraints are applied at all n atmospheric exits:

$$\left.\begin{aligned} t_{\text{exit},\,i} &= t_i^- \\ h(t_{\text{exit},\,i}) &= 60\ \text{nm} \\ h(t_{\text{exit},\,i}) &= h(t_i^-) \\ \theta(t_{\text{exit},\,i}) &= \theta(t_i^-) \\ \phi(t_{\text{exit},\,i}) &= \phi(t_i^-) \\ v(t_{\text{exit},\,i}) &= v(t_i^-) \\ \gamma(t_{\text{exit},\,i}) &= \gamma(t_i^-) \\ \psi(t_{\text{exit},\,i}) &= \psi(t_i^-) \end{aligned}\right\}, \quad i = 1, \ldots, n \tag{17}$$

To ensure that the vehicle can reach the next intermediate apogee, the flight path angle must be positive at all n atmospheric exits. Consequently, the following inequality constraint is applied at all n atmospheric exits:

$$\gamma(t_{\text{exit},\,i}) \geqslant 0, \quad i = 1, \ldots, n \tag{18}$$

Furthermore, let the times of the applications of the intermediate impulses $\Delta V_2, \ldots, \Delta V_n$ be denoted $t_{\text{int},2}, \ldots, t_{\text{int},n}$, respectively. To ensure that the intermediate impulses are applied at apogee, the following equality constraint is applied at the termination of each of the space flight segments s_i^-, $i = 2, \ldots, n$:

$$\gamma(t_{\text{int},\,i}) = 0, \quad i = 2, \ldots, n \tag{19}$$

Finally, denoting the terminal time by t_{f}, the following equality constraints are applied immediately after the application of the impulse ΔV_{n+1}:

$$\left.\begin{aligned} r(t_{\text{f}}) &= h_{\text{f}} + R_{\text{e}} \\ v(t_{\text{f}}) &= \sqrt{\frac{\mu}{r_{\text{f}}}} \\ \gamma(t_{\text{f}}) &= 0 \\ i(t_{\text{f}}) &= i_{\text{f}} \end{aligned}\right. \tag{20}$$

where h_{f} corresponds to the altitude of the desired terminal circular low Earth orbit and i_{f} is the desired terminal inclination.

OPTIMAL CONTROL PROBLEM

The optimal control problem is now stated formally. Using the event sequence of the previous subsection, find the set of admissible controls $(u_1, u_2) \in \mathscr{U}$ and the parameters

$$\Delta V_i, \quad i = 1, \ldots, n+1$$
$$\chi_i, \quad i = 1, \ldots, n$$
$$\Delta\tau_i^-, \quad i = 2, \ldots, n+1$$
$$\Delta\tau_i^+, \quad i = 1, \ldots, n$$

that minimize the objective functional

$$J \equiv \Delta V = \sum_{i=1}^{n+1} \Delta V_i \tag{21}$$

subject to the differential constraint of Equation (11), the path constraints of Equations (8) and (9), the initial condition of Equation (14), the interior point constraints of Equations (16)–(19), and the terminal constraint of Equation (20).

NUMERICAL OPTIMIZATION

The multiple-pass aeroassisted orbital transfer optimal control problem described in the previous section is solved using the direct transcription program *Sparse Optimal Control Software* (SOCS) [15]. SOCS transcribes the optimal control problem to a non-linear programming (NLP) problem and solves the NLP using the sparse non-linear optimizer SPRNLP [24]. A description of direct transcription methods is beyond the scope of this paper, but details can be found in [13, 14, 25].

The procedure for using SOCS is as follows. It is necessary to specify an initial node distribution (mesh), i.e. an initial set of time points at which to compute the optimal solution, for each phase of the problem. Furthermore, at each node it is necessary to specify a guess for the state and control and for each phase it is necessary to specify a guess for the optimization parameters. Finally, it is necessary to specify differential equation accuracy tolerances and optimization convergence tolerances. The optimal solution is then computed using all of the aforementioned information. If, upon convergence, the differential equation accuracy tolerance is not met, a mesh refinement strategy is invoked that adds nodes to form a denser mesh; the optimization problem is then solved on the refined mesh. This process of solving the optimization problem and refining the mesh is repeated until the user-specified accuracy tolerances are met. A schematic of the aforementioned procedure is shown in Figure 4.

Due to the complexity of this problem, it was a great challenge to determine initial guesses for the trajectory and the optimization parameters. Before proceeding to the multiple-pass transfer, initial guesses were determined for the one-pass transfer as follows. The impulse ΔV_1 and change in true anomaly $\Delta\tau_1^+$ were chosen such that the initial space flight segment would terminate at an altitude of 60 nm (the initial yaw angle χ_1 was set to zero). Then, using the state at the end of the

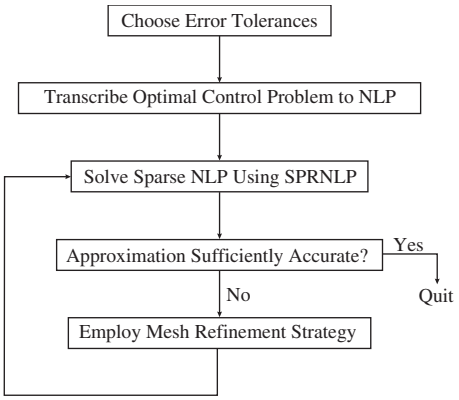

Figure 4. Schematic of the procedure used by SOCS.

initial space flight segment, an atmospheric trajectory was simulated using a control (u_1, u_2) such that the vehicle would descend into the atmosphere and subsequently re-attain an altitude of 60 nm with a positive flight path angle. Finally, using the state at the end of the atmospheric flight segment, a change in true anomaly $\Delta\tau_2^-$ and a circularizing impulse ΔV_2 were chosen such that the vehicle terminated in a circular orbit. Using this initial guess, the one-pass transfer was then optimized for various desired final inclinations.

The initial guesses for all n-pass transfers ($n > 1$) were determined using a bootstrap procedure based on the optimized $(n-1)$-pass transfers. The bootstrap procedure was setup as follows. The impulses $\Delta V_1, \ldots, \Delta V_{n-1}, \Delta V_{n+1}$, the yaw angles $\Delta\chi_1, \ldots, \Delta\chi_{n-1}$, and the changes in true anomaly $\Delta\tau_2^-, \ldots, \Delta\tau_{n-1}^-, \Delta\tau_{n+1}^-, \Delta\tau_1^+, \ldots, \Delta\tau_{n-1}^+$, were taken from the optimized $(n-1)$-pass transfer whose final inclination was the same as the desired final inclination of the corresponding n-pass transfer. The impulse ΔV_n and yaw angle $\Delta\chi_n$ were chosen arbitrarily as 100 ft/s and 0°, respectively. Similarly, the guesses for the trajectories and controls for atmospheric flight segments $1, \ldots, n-1$ were taken from the optimized $(n-1)$-pass transfer whose final inclination was the same as the desired final inclination for the n-pass transfer. The trajectories and controls for the nth atmospheric flight segment were set equal to those of the $(n-1)$th atmospheric flight segment of the optimized $(n-1)$-pass transfer whose final inclination was the same as the desired final inclination of the corresponding n-pass transfer. The changes in true anomaly $\Delta\tau_n^-$, and $\Delta\tau_n^+$ were chosen such that the space flight segment s_n^- terminated at apogee and the space flight segment s_n^+ terminated at an altitude of 60 nm. Each n-pass transfer was then optimized using the appropriate initial guess.

RESULTS

The multiple-pass aeroassisted orbital transfer optimal control problem described in the previous section was solved using SOCS for $n = (1, \ldots, 9)$, $\dot{Q}_{\max} = (2000, 1000, 600, 500, 400)$ BTU/(ft^2 s), and $i_f = (50, 70, 89)$ degrees from the initial condition of Equation (14) to a final circular orbit of 100 nm. The heating rate constraint was active for all cases except $\dot{Q}_{\max} = 2000$

BTU/(ft^2 s), i.e. the case $\dot{Q}_{\max} = 2000$ BTU/(ft^2 s) was equivalent to a problem with no constraint on $\dot{Q}$.

The minimum total impulse, $\Delta V_{\min}$, is shown in Figures 5–7 as a function of n for the different values of $\dot{Q}_{\max}$. When the heating rate is unconstrained the multiple-pass transfer offers only a

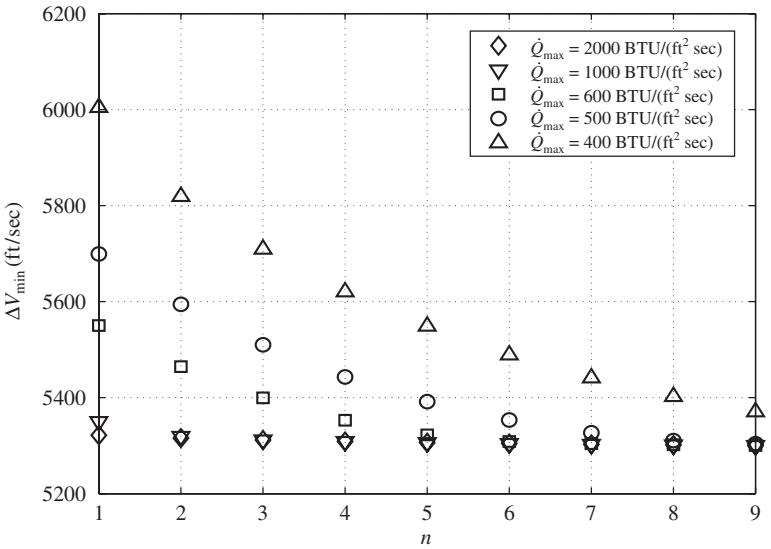

Figure 5. $\Delta V_{\min}$ vs n for $i_f = 50^\circ$.

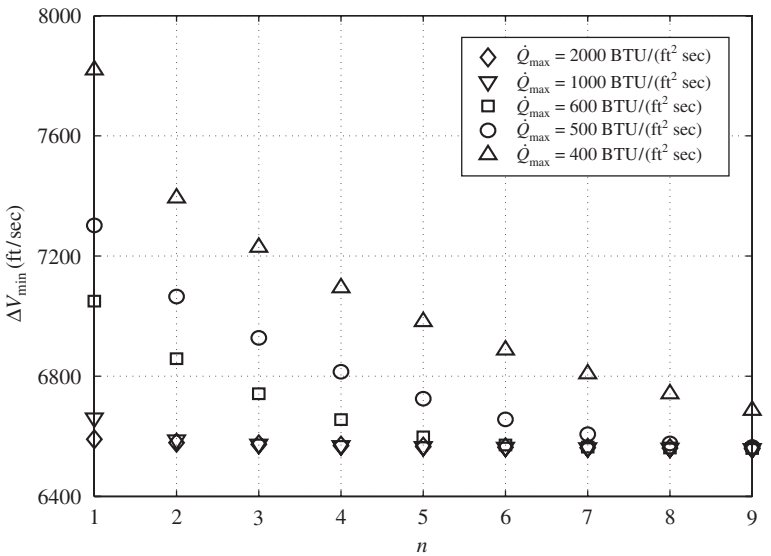

Figure 6. $\Delta V_{\min}$ vs n for $i_f = 70^\circ$.

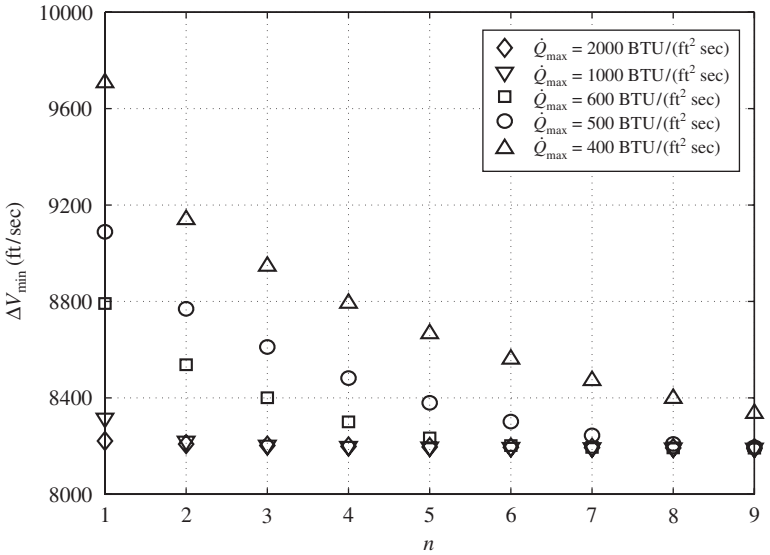

Figure 7. $\Delta V_{\min}$ vs n for $i_f = 89^\circ$.

small savings in ΔV over the single-pass transfer whereas when the heating rate is constrained the multiple-pass maneuver offers significant savings in ΔV over the single-pass transfer. Moreover, this savings in $\Delta V_{\min}$ increases as $\dot{Q}_{\max}$ decreases. Finally, the advantage of adding atmospheric passes diminishes as n increases.

An interesting feature of all computed optimal trajectories is that the intermediate impulses were very small in magnitude (0.87 ft/s or less) and contributed less than 5 ft/s to the total impulse. These observations suggest that the optimal trajectories would not be affected significantly if the intermediate impulses were eliminated altogether. This hypothesis was verified by solving a modified optimal control problem where the intermediate impulses were set to zero. In all cases the difference between the optimal objective functionals for the original and modified optimal control problems were small (less than 5 ft/s) and the corresponding optimal trajectories were essentially identical. It is noted for completeness that in a real flight it would be necessary to employ small intermediate impulses as mid-course corrections to set up the next atmospheric pass.

Another feature of the optimal trajectories is the split between atmospheric inclination change and impulsive inclination change. Figures 8–10 show the total atmospheric inclination change, Δi_{aero}, as a function of n for the different values of $\dot{Q}_{\max}$. Similar to the results for $\Delta V_{\min}$, the value of Δi_{aero} approaches a constant geometrically as n increases. Interestingly, this limit of approximately 36.2° is independent of i_f which indicates that, beyond a certain threshold (in this case $n \approx 9$), adding atmospheric passes does not increase Δi_{aero}. This limit is most likely due to a limit on the achievable atmospheric plane change caused by the lift-to-drag ratio of the vehicle. Moreover, because the intermediate impulses are essentially zero, all of the impulsive inclination change is accomplished with the initial de-orbit impulse, ΔV_1.

A key issue when performing a multiple-pass aeroassisted orbital transfer is the overall transfer time. Figures 11–13 show the transfer time, T, as a function of n for the different

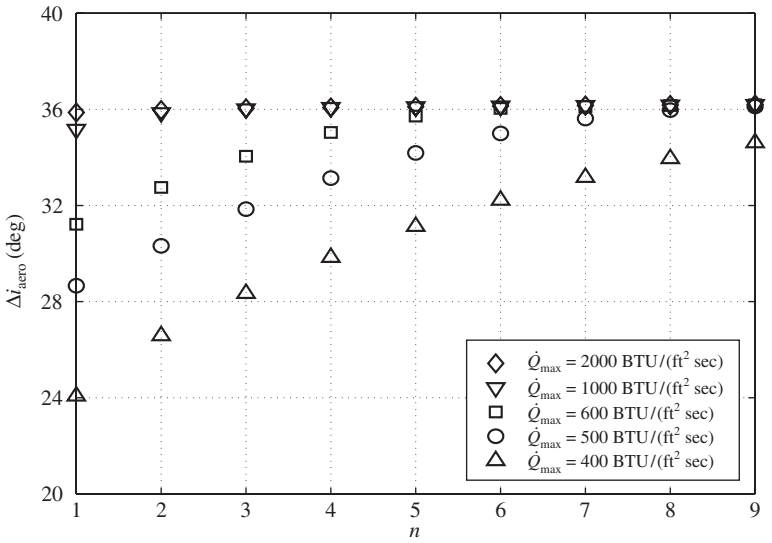

Figure 8. Total atmospheric inclination change, Δi_{aero} vs n for $i_{\text{f}} = 50^{\circ}$.

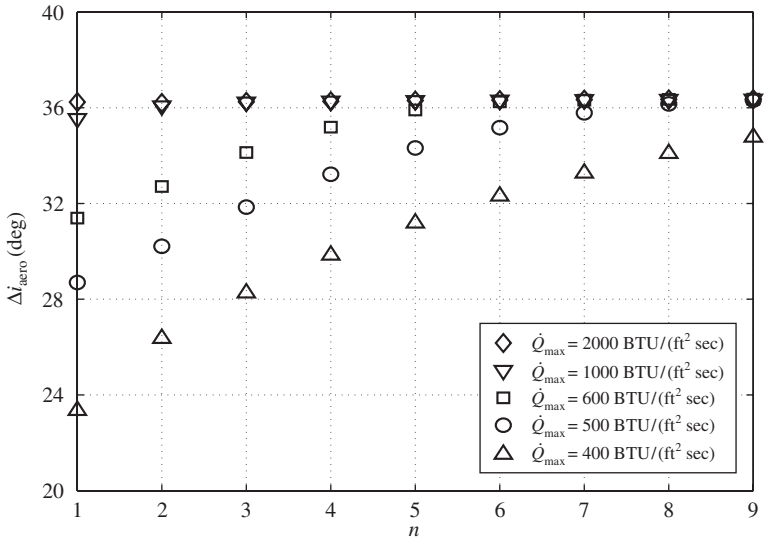

Figure 9. Total atmospheric inclination change, Δi_{aero} vs n for $i_{\text{f}} = 70^{\circ}$.

values of $\dot{\boldsymbol{Q}}_{\max}$. It is seen for all cases that the transfer time for $n = 1$ is approximately 6 h. Furthermore, for a particular value of n the transfer time is the shortest when $\dot{Q}$ is unconstrained.

One of the purported advantages of aeroassisted orbital transfer is the savings in required impulse over non-coplanar two-impulse (Hohmann-type) and three-impulse (bi-elliptic) all-propulsive transfers [26]. Table II shows the minimum ΔV requirements for these all-propulsive

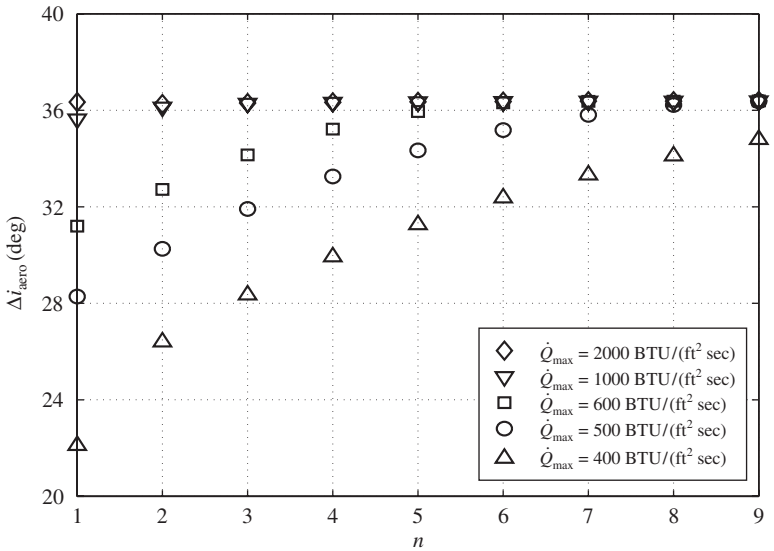

Figure 10. Total atmospheric inclination change, Δi_{aero} vs n for $i_{\text{f}} = 89^\circ$.

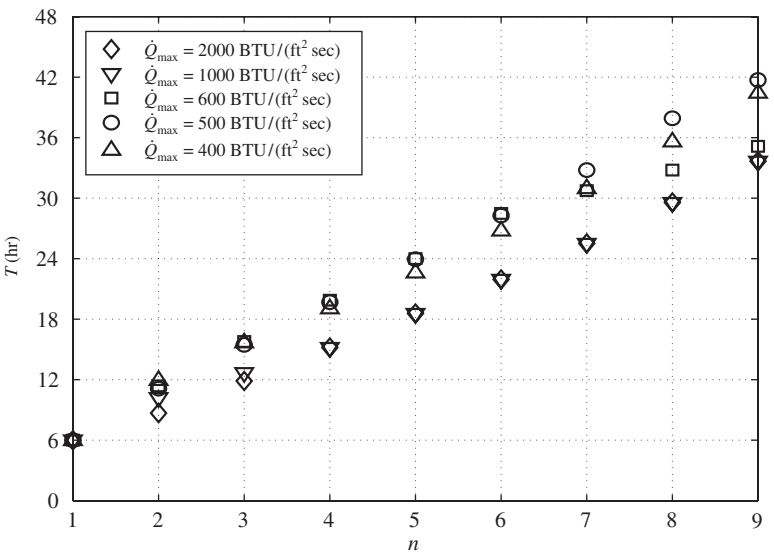

Figure 11. Transfer time, T vs n for $i_{\text{f}} = 50^\circ$.

transfers from GEO to 100 nm altitude circular orbit for final inclinations of 50, 70, and 89° (the three impulse bielliptic transfer were constrained to be less than 300 days). It can be seen in all cases that the aeroassisted orbital transfer offers substantial savings in ΔV over either of these all-propulsive transfers.

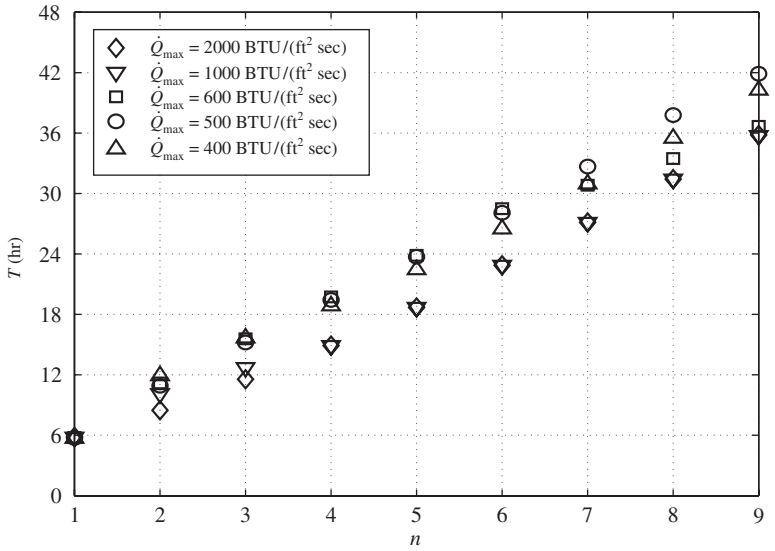

Figure 12. Transfer time, T vs n for $i_f = 70^\circ$.

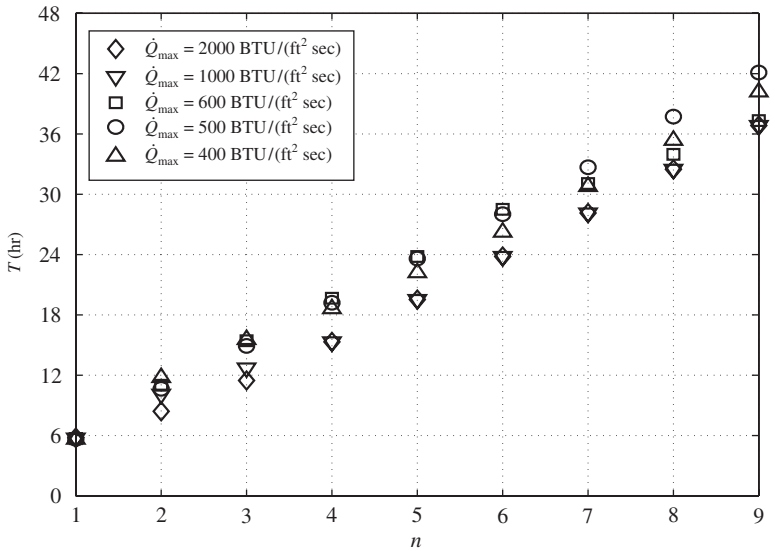

Figure 13. Transfer time, T vs n for $i_f = 89^\circ$.

The case $n = 4$, $\dot{Q}_{max} = 400$ BTU/(ft^2 s), and $i_f = 89^\circ$ is now used to illustrate the main features common to all of the computed optimal trajectories. Results for h, v, and i are shown in Figures 14 and 15. It can be seen that the speed at each atmospheric exit is equal to the speed at the subsequent atmospheric entry. This behaviour is expected since the entry and exit altitudes

Table II. Results of two-impulse and three-impulse all-propulsive transfers from GEO to 100 nm circular orbit for $i_f = 50$, 70, and 89°

i_f (deg)	ΔV (ft/s) (two-burn)	ΔV (ft/s) (three-burn)
50	15 800	14 795
70	17 600	14 820
89	19 260	14 840

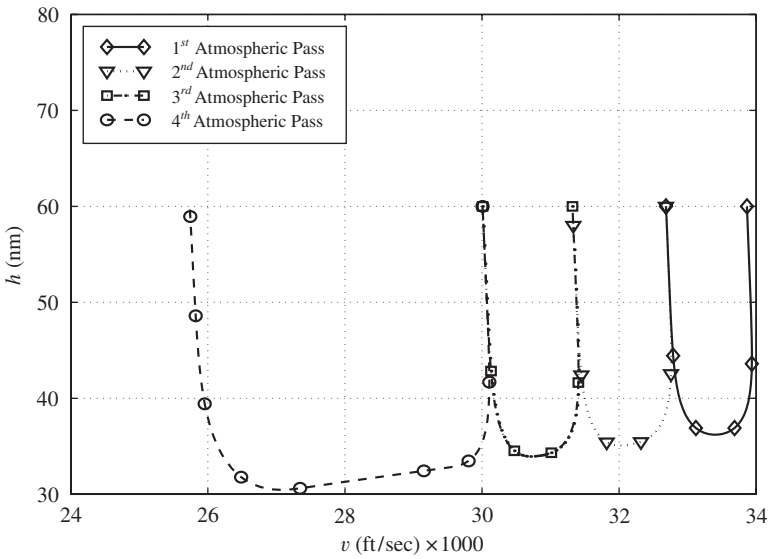

Figure 14. h vs v for $n = 4$, $\dot{Q}_{max} = 400\,\text{BTU}/(\text{ft}^2\,\text{s})$, and $i_f = 89°$.

are equal and there is essentially no change to the Keplerian orbit during the intervening space flight segment. Moreover, the decrease in speed during the final atmospheric pass is significantly larger than the decrease in speed during any of the earlier atmospheric passes. The reason for this larger speed decrease is that the velocity is lowest during the final atmospheric pass and thereby permits deeper atmospheric penetration. Similarly, the inclination at atmospheric exit and the subsequent atmospheric entry are equal and the inclination change during the last atmospheric pass is significantly larger than the inclination change during any of the earlier atmospheric passes.

Results for γ are shown in Figure 16. A structure common to all optimal trajectories is that h is nearly symmetric with respect to γ for all but the final atmospheric pass. During the final atmospheric flight segment it is seen that two flight conditions occur simultaneously. First, the vehicle achieves an altitude change at constant flight path angle. Second, (see Figure 20) the vehicle flies along its heating rate limit. These two flight conditions together demonstrate that, during the final atmospheric segment, the vehicle is flying along an *equilibrium glide* condition.

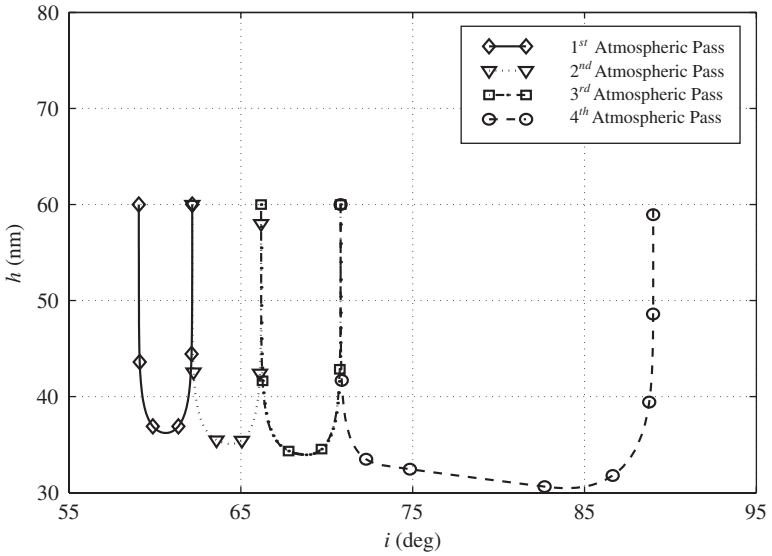

Figure 15. h vs i for $n = 4$, $\dot{Q}_{\max} = 400\,\mathrm{BTU/(ft^2\,s)}$, and $i_f = 89^\circ$.

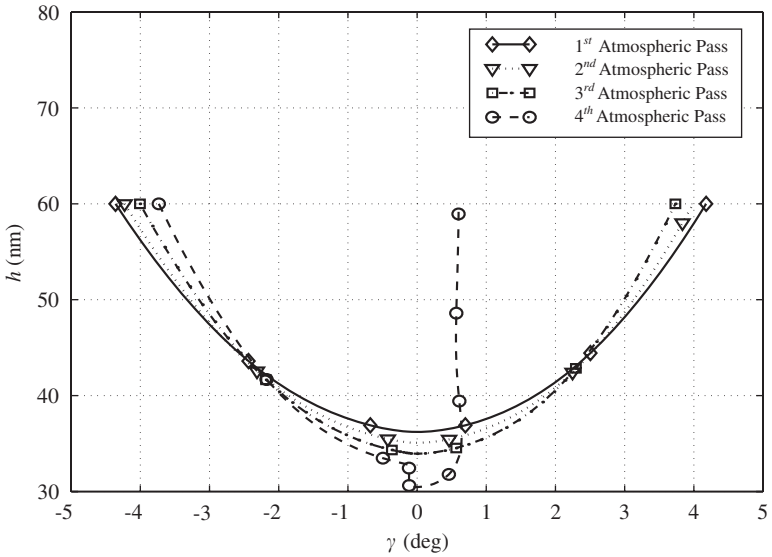

Figure 16. h vs γ for $n = 4$, $\dot{Q}_{\max} = 400\,\mathrm{BTU/(ft^2\,s)}$, and $i_f = 89^\circ$

The equilibrium glide condition during the final atmospheric flight segment was common to all of the optimal trajectories.

Typical control profiles σ and C_L are shown in Figures 17–19. It can be seen from Figure 19 that the constraint on C_L is active during the entirety of the first atmospheric flight segment.

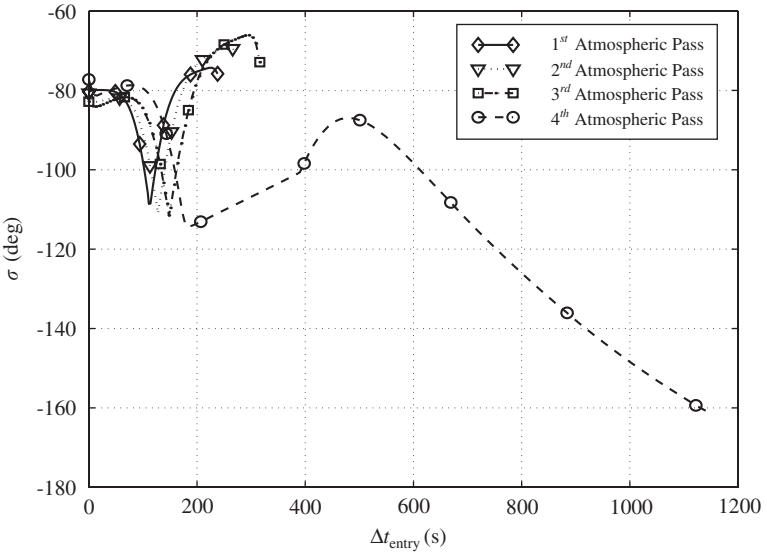

Figure 17. σ vs Δt_{entry} for $n = 4$, $\dot{Q}_{\max} = 400\,\text{BTU}/(\text{ft}^2\,\text{s})$, and $i_{\text{f}} = 89^\circ$.

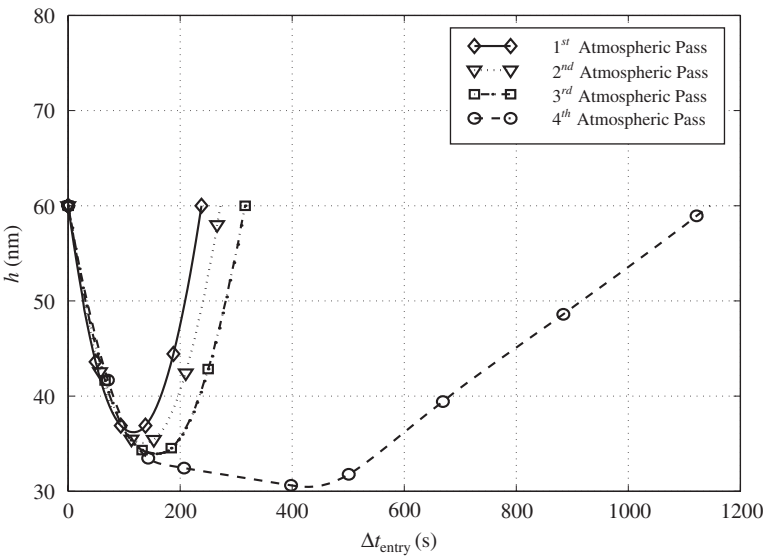

Figure 18. h vs Δt_{entry} for $n = 4$, $\dot{Q}_{\max} = 400\,\text{BTU}/(\text{ft}^2\,\text{s})$, and $i_{\text{f}} = 89^\circ$.

Furthermore, it can be seen by examining Figures 17 and 18 simultaneously that a reversal in bank angle rate always occurs when the vehicle reaches a minimum altitude.

The value of $\dot{Q}$ is shown in Figure 20 where $\dot{Q}$ is plotted alongside the time from atmospheric entry, Δt_{entry}. It can be seen that $\dot{Q}$ rides the path constraint upper bound during the final

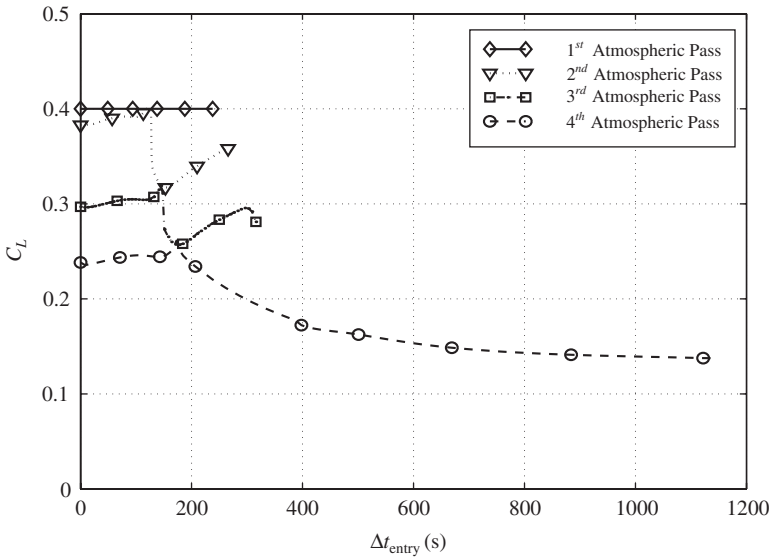

Figure 19. C_{L} vs Δt_{entry} for $n = 4$, $\dot{Q}_{\max} = 400\,\text{BTU}/(\text{ft}^2\,\text{s})$, and $i_{\text{f}} = 89^\circ$.

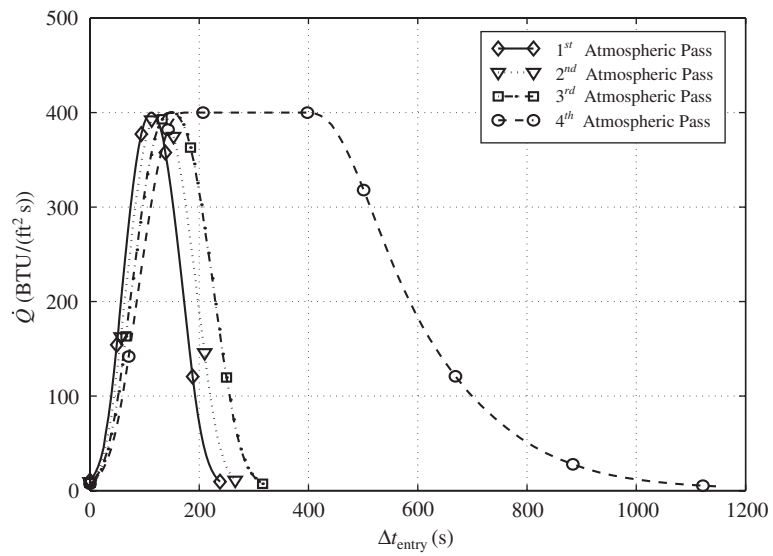

Figure 20. $\dot{Q}$ vs Δt_{entry} for $n = 4$, $\dot{Q}_{\max} = 400\,\text{BTU}/(\text{ft}^2\,\text{s})$, and $i_{\text{f}} = 89^\circ$.

atmospheric flight segment but appears to only touch the constraint during all earlier atmospheric flight segments. While the conditions derived in Reference [27] can be used to rule out the existence of a touch point in the current application, a rigorous analysis is beyond the scope of this paper.

CONCLUSIONS

A numerical optimization study of multiple-pass aeroassisted orbital transfer has been performed using a direct transcription method. The objective has been to provide highly accurate solutions to the problem of minimum-impulse heat-rate-limited large plane change multiple-pass aerogliding maneuvers for a high lift-to-drag vehicle from geostationary orbit to low Earth orbit. The minimum-impulse performance has been assessed as a function of the number of atmospheric passes, the maximum allowable heating rate, and the desired terminal inclination.

The results show that the multiple-pass aeroassisted orbital transfer offers little to no savings in total impulse over the single-pass transfer when the heating rate is unconstrained but offers significant savings in total impulse when the heating rate is constrained. A useful feature of the approach developed here is that the optimal split between atmospheric and impulsive inclination change is determined. Furthermore, it was found that there is a limit to the total amount of inclination change performed during atmospheric flight. Finally, a particular case of a four-pass transfer was used to illustrate the main features common to all of the optimal trajectories.

NOMENCLATURE

C_D	coefficient of drag
C_{D_0}	zero-lift coefficient of drag
C_L	coefficient of lift
$C_{L,\alpha}$	derivative of C_L with respect to α, deg^{-1}
$C_{L,\max}$	maximum coefficient of lift
D	drag acceleration, ft/s^2
g_0	gravitational acceleration at sea level, ft/s^2
h	altitude, ft and nm
h_a	apogee altitude, nm
h_f	altitude of spacecraft in final circular orbit, ft and nm
h_p	perigee altitude, nm
i	inclination, deg
I_{sp}	specific impulse, s
K	drag polar parameter
L	lift acceleration, ft/s^2
m	vehicle mass, slug
m_0	initial vehicle mass, slug
m_e	final vehicle mass, slug
q	dynamic pressure, lb/ft^2
$\dot{Q}$	heating rate, $\text{BTU/(ft}^2\text{ s)}$
$\dot{Q}_{\max}$	maximum stagnation point heating rate, $\text{BTU/(ft}^2\text{ s)}$
r	radius, ft
$\boldsymbol{r}$	inertial position, ft
R_e	radius of Earth, ft
S	vehicle reference area, ft^2

s^-	space flight segment before impulsive maneuver
s^+	space flight segment after impulsive maneuver
t	time, s
T	orbital transfer time, s
$\boldsymbol{v}$	inertial velocity, ft/s
v	speed, ft/s
v_e	circular orbit speed at surface of the Earth, ft/s
α	angle of attack, deg
α_{max}	maximum angle of attack, deg
χ	Euler yaw angle of impulsive thrust maneuver, ft/s
Δt_{entry}	Time since atmospheric entry, s
ΔV	magnitude of impulsive thrust maneuver, deg
$\Delta\tau$	change in true anomaly, deg
γ	flight path angle, deg
μ	gravitational parameter, ft^3/s^2
ν	true anomaly, deg
ω	argument of perigee, deg
Ω	right ascension of ascending node, deg
θ	longitude angle, deg
ψ	heading angle, deg
ρ	air density, $slug/ft^3$
ρ_e	air density at sea level, $slug/ft^3$
σ	bank angle, deg
ϕ	latitude angle, deg
τ	true anomaly, deg

ACKNOWLEDGEMENTS

The authors gratefully acknowledge the United States Air Force Space and Missile Systems Center for supporting this research. Furthermore, the authors acknowledge Twain Summerset for his role as technical monitor and his helpful insights throughout the course of this work. Finally, the authors acknowledge Alan Jenkin, Steven Hast, and Ryan Noguchi of The Aerospace Corporation for their helpful comments and suggestions in preparing this manuscript.

REFERENCES

1. Walberg GD. A survey of aeroassisted orbit transfer. *Journal of Spacecraft and Rockets* 1985; **22**(1):3–17.
2. Mease KD. Optimization of aeroassisted orbital transfer: current status. *Journal of the Astronautical Sciences* 1988; **36**(1/2):7–33.
3. Hull DG, Giltner JM, Speyer JL, Mapar J. Minimum energy-loss guidance for aeroassisted orbital plane change. *Journal of Guidance, Control, and Dynamics* 1985; **8**(4):487–493.
4. Melamed N, Calise AJ. Evaluation of an optimal-guidance for an aero-assisted orbit transfer. *Journal of Guidance, Control, and Dynamics* 1995; **18**(4):718–722.
5. Seywald H. Variational solutions for the heat-rate-limited aeroassisted orbital transfer problem. *Journal of Guidance, Control, and Dynamics* 1996; **19**(3):686–692.
6. Lee JY, Hull DG. Maximum orbit plane change with heat-transfer-rate considerations. *Journal of Guidance, Control, and Dynamics* 1990; **13**(3):492–497.
7. Vinh NX, Hanson JM. Optimal aeroassisted return from high earth orbit with plane change. *Acta Astronautica* 1985; **12**(1):11–25.

8. Vinh NX, Ma D-M. Optimal multiple-pass aeroassisted plane change. *Acta Astronautica* 1990; **21**(11/12):749–758.
9. Hargraves CR, Paris SW. Direct trajectory optimization using nonlinear programming and collocation. *Journal of Guidance, Control, and Dynamics* 1987; **10**(4):338–342.
10. Enright PJ, Conway BA. Optimal finite-thrust spacecraft trajectories using collocation and nonlinear programming. *Journal of Guidance, Control, and Dynamics* 1991; **14**(5):981–985.
11. Herman AL, Conway BA. Direct optimization using collocation based on high-order gauss-lobatto quadrature rules. *Journal of Guidance, Control, and Dynamics* 1996; **19**(3):592–599.
12. Betts JT. Survey of numerical methods for trajectory optimization. *Journal of Guidance, Control, and Dynamics* 1998; **21**(2):193–207.
13. Vlases WG, Paris SW, Lajoie RM, Martens PJ, Hargraves CR. Optimal trajectories by implicit simulation. *Boeing Aerospace and Electronics, Technical Report WRDC-TR*-90-3056, Wright-Patterson Air Force Base, 1990.
14. Schnepper K. PROMIS Software User Manual. Schwerpunktprogramm der Deutschen Forschungsgemeinschaft: Andwendungsbezogene Optimierung and Steuerung, Report 509, Institute of Flight Mechanics and Control, University of Stuttgart, Stuttgart, Germany, 1994.
15. Betts JT, Huffman WP. Sparse optimal control software, SOCS. *Mathematics and Engineering Analysis Library Report*. MEA-LR-085, 15 July 1997, Boeing Information and Support Services, P.O. Box 3797, Seattle, WA, 98124-2297.
16. Zimmermann F, Calise AJ. Numerical optimization study of aeroassisted orbital transfer. *Journal of Guidance, Control and Dynamics* 1998; **21**(1):127–133.
17. Hanson JM. Combining propulsive and aerodynamic maneuvers to achieve optimal orbital transfer. *Journal of Guidance, Control, and Dynamics* 1985; **12**(5):732–738.
18. Huffman WP. An analytic propagation method for low earth orbits. *Internal Document*. The Aerospace Corporation, El Segundo, CA, November 1981.
19. Vinh NX, Busemann A, Culp RD. Hypersonic and planetary entry flight mechanics. University of Michigan Press, Ann Arbor, MI, 1980.
20. Brenan KE. A Smooth Approximation to the GTS 1962 Standard Atmosphere Model. Aerospace ATM 82-(2468-04)-7, 21 May 1982.
21. Detra RW, Kemp NH, Riddell FR. Addendum to heat transfer to satellite vehicles re-entering the atmosphere. *Jet Propulsion* 1957; **27**:1256–1257.
22. Brenan KE, Campbell SL, Petzold JR. *Numerical Solution of Initial-Value Problems in Differential Algebraic Equations*. Elsevier Sciences Publishing: New York, 1989.
23. Brenan KE. Differential-algebraic equations issues in the direct transcription of path constrained optimal control problems. *Annals of Numerical Mathematics* 1994; **1**:247–263.
24. Betts JT, Frank PD. A sparse nonlinear optimization algorithm. *Journal of Optimization Theory and Applications* 1994; **82**(3):519–541.
25. Jansch C, Schnepper K, Well, K. Multi-phase trajectory optimization methods with applications to hypersonic vehicles. Schwerpunktprogramm der Deutchen Forschungsgemeinschaft: Anwendungsbezogene Optimierung and Steuerung, Report 419, Institute of Flight Mechanics and Control, University of Stuttgart, Stuttgart, Germany, 1994.
26. Chobotov VA. *Orbital Mechanics*. American Institute of Aeronautics and Astronautics: Washington, DC, 1991.
27. Seywald H, Cliff EM. On the existence of touch points for first-order state inequality constraints. *Optimal Control Applications and Methods* 1996; **17**:357–366.

